ORIGINAL PAPER

Fluorescence Studies on New Potential Antitumoral Benzothienopyran-1-ones in Solution and in Liposomes

Elisabete M. S. Castanheira · M. Solange D. Carvalho · Daniel J. G. Soares · Paulo J. G. Coutinho · Ricardo C. Calhelha · Maria-João R. P. Queiroz

Abstract Fluorescence properties of four new potential antitumoral compounds, 3-arylbenzothieno[2,3-*c*]pyran-1-ones, were studied in solution and in lipid membranes of dipalmitoyl phosphatidylcholine (DPPC), egg yolk phosphatidylcholine (Egg-PC) and dioctadecyldimethylammonium bromide (DODAB). The 3-(4-methoxyphenyl)benzothieno [2,3-*c*]pyran-1-one (**1c**) exhibits the higher fluorescence quantum yields in all solvents studied. All compounds present a solvent sensitive emission, with significant red shifts in polar solvents for the methoxylated compounds. The results point to an ICT character of the excited state, more pronounced for compound **1c**. Fluorescence (steady-state) anisotropy measurements of the compounds incorporated in liposomes of DPPC, DODAB and Egg-PC indicate that all compounds have two different locations, one due to a deep penetration in the lipid membrane and another corresponding to a more hydrated environment. In general, the methoxylated compounds prefer hydrated environments inside the liposomes. The 3-(4-fluorophenyl)benzothieno[2,3-*c*]pyran-1-one (**1a**) clearly prefers a hydrated environment, with some molecules located at the outer part of the liposome interface. On the contrary, the preferential location of 3-(2-fluorophenyl)benzothieno[2,3-*c*] pyran-1-one (**1b**) is in the region of lipid hydrophobic tails. Compounds with a planar geometry (**1a** and **1c**) have higher mobility in the lipid membranes when phase transition occurs.

E. M. S. Castanheira (✉) · M. S. D. Carvalho · D. J. G. Soares · P. J. G. Coutinho
Centro de Física (CFUM), Universidade do Minho,
Campus de Gualtar,
4710-057 Braga, Portugal
e-mail: ecoutinho@fisica.uminho.pt

M. S. D. Carvalho · R. C. Calhelha · M.-J. R. P. Queiroz
Centro de Química (CQ-UM), Universidade do Minho,
Campus de Gualtar,
4710-057 Braga, Portugal

Abbreviations

DPPC	Dipalmitoyl phosphatidylcholine
DODAB	Dioctadecyldimethylammonium bromide
Egg-PC	Egg yolk phosphatidylcholine
PC	Phosphatidylcholine

Introduction

Our research group has been interested in the synthesis and in the photophysical behavior, in solution and in lipid membranes, of novel heteroaromatic biological active compounds [1–3].

Recently, some of us have described the synthesis of new 3-(aryl)benzothieno[2,3-*c*]pyran-1-ones from 3-bromobenzo [*b*]thiophene-2-carboxylic acid and different arylphenylacetylenes [4] (compounds **1a–c**, Fig. 1). Compound **1d**, with a methoxy group in the *ortho* position relative to the pyranone ring (Fig. 1) was synthesized in this work (Scheme 1) for comparison, and the synthesis is described below.

Compounds **1a–c** were evaluated for their capacity to inhibit the in vitro growth of three human tumor cell lines, MCF-7 (breast adenocarcinoma), NCI-H460 (non-small cell lung cancer) and SF-268 (CNS cancer). Compound **1b** was shown to be the most potent against the three cell lines tested, presenting low GI_{50} (the lowest concentration causing 50% of the cell growth inhibition after a continuous exposure of 48 h) values (12–19 µM) [4].

These results suggested us to perform fluorescence studies of compounds **1a–d** incorporated in liposomes. The photophysical properties in solution and in lipid vesicles of DPPC (dipalmitoyl phosphatidylcholine), Egg-PC (egg yolk phosphatidylcholine) and of the cationic lipid DODAB (dioctadecyldimethylammonium bromide) were studied. The

phospholipids DPPC and phosphatidylcholine (from egg yolk) are neutral components of biological membranes, while cationic liposomes based in DODAB have been used as vehicles for DNA transfection and drug delivery [5–7]. Fluorescence (steady-state) anisotropy measurements were also performed to obtain further information about the location of these compounds in lipid membranes.

Experimental

Synthesis

General The melting point (°C) was determined on a SMP3 Stuart apparatus. ^{1}H and ^{13}C NMR spectra were recorded on a Bruker Avance II$^+$ at 400 and 100.6 MHz, respectively. Chemical shifts (δ) are given in ppm. MS (EI) spectrum and HRMS on the M$^+$ were recorded by the mass spectrometry service of the University of Vigo, Spain. Petroleum ether refers to the boiling range 40–60 °C.

3-(2-methoxyphenyl)benzothieno[2,3-c]pyran-1-one (1d) 3-Bromo-benzo[*b*]thiophene-2-carboxylic acid (100 mg, 0.390 mmol), 2-methoxyphenylacetylene (1.2 equiv.) PdCl$_2$(PPh$_3$)$_2$ (5 mol%), CuI (3 mol%), and NEt$_3$ (3 equiv.) were added under argon to dry DMF (2 mL) in a dry Schlenk tube and the mixture was heated for 2 h at 100 °C. After cooling, water (5 mL) and ethyl acetate (5 mL) were added and the phases were separated. The aqueous phase

was then extracted with more ethyl acetate (3×5 mL) and the organic phases were collected, dried (MgSO$_4$) and filtered. The solvent removal gave a solid which was crystallized from CH$_2$Cl$_2$/petroleum ether affording **1d** as a beige solid (95 mg, 80%), m.p. 191–193 °C. ^{1}H-NMR (400 MHz, DMSO-d_6) δ 3.98 (3H, s, OMe), 7.11–7.15 (1H, m, ArH), 7.23–7.25 (1H, m, ArH), 7.48–7.53 (1H, m, ArH), 7.62–7.66 (1H, m, ArH), 7.70–7.74 (1H, m, ArH), 7.80–7.83 (1H, m, ArH), 7.99 (1H, s, 4-H), 8.21–8.24 (1H, m, ArH), 8.43–8.45 (1H, m, ArH) ppm. ^{13}C-NMR (100.6 MHz, DMSO-d_6) δ 55.30 (OCH$_3$), 101.83 (CH), 112.26 (CH), 120.02 (C), 120.73 (CH), 121.20 (C), 123.92 (CH), 124.69 (CH), 125.79 (CH), 128.63 (CH), 129.61 (CH), 131.69 (CH), 134.10 (C), 142.46 (C), 144.07 (C), 154.26 (C), 157.06 (C), 158.08 (C) ppm. MS (EI): m/z 308 (M$^+$, 100), 280 (M$^+$-28, 59). HRMS M$^+$ calc. for C$_{18}$H$_{12}$O$_3$S: 308.0507, found: 308.0508.

Spectroscopic studies

Materials and methods

All the solutions were prepared using spectroscopic grade solvents and ultrapure water (Milli-Q grade). 1,2-Dipalmitoyl-*sn*-glycero-3-phosphocholine (DPPC) and 1,2-Diacyl-*sn*-glycero-3-phosphocholine from egg yolk (Egg-PC), from Sigma-Aldrich, and dioctadecyldimethylammonium bromide (DODAB), from Tokyo Kasei, were used as received (lipid structures are shown below).

DPPC
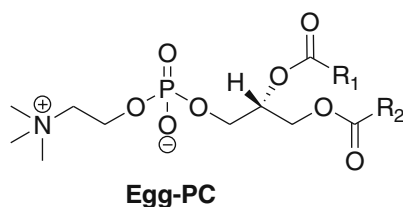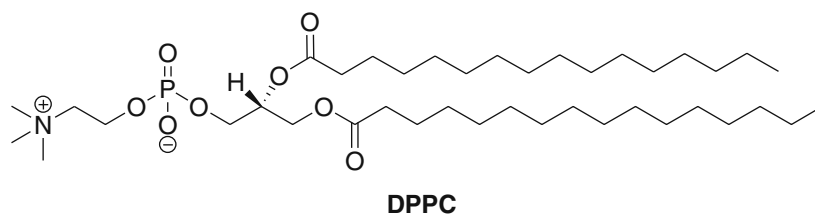
Egg-PC

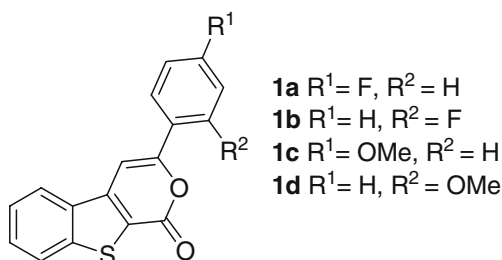R$_1$, R$_2$ = fatty acid residues

DODAB
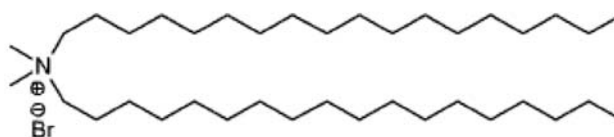
Fig. 1 Structure of 3-(aryl)benzothieno[2,3-*c*]pyran-1-ones

For Egg-PC vesicles preparation, defined volumes of a stock solution of lipid (34.5 mM) and compound (0.2 mM) in ethanol were injected together, under vigorous stirring, to an aqueous buffer solution (10 mM Tris, pH=7.4), at room temperature. A similar procedure was adopted for DPPC and DODAB liposomes, but the injection of the required amounts of stock solutions of lipid (50 mM for DPPC and 20 mM for DODAB) and compound in ethanol was done at 60 °C, well above the melting transition temperature of both lipids, *ca.* 41 °C for DPPC [8] and 45 °C for DODAB [9]. In all cases, the final lipid concentration was 1 mM, with compounds **1a**–**d**/lipid molar ratio of 1:500.

Spectroscopic measurements

Absorption spectra were recorded in a Shimadzu UV-3101PC UV-Vis-NIR spectrophotometer. Fluorescence measurements were performed using a Spex Fluorolog 3 spectrofluorimeter, equipped with double monochromators in both excitation and emission, Glan-Thompson polarizers and a temperature-controllable cuvette holder. Fluorescence spectra were corrected for the instrumental response of the system.

For fluorescence quantum yield determination, the solutions were previously bubbled for 20 min with ultrapure nitrogen. The fluorescence quantum yields (Φ_s) were determined using the standard method (Eq. 1) [10, 11]. Anthracene in ethanol (Φ_r=0.27 at 25 °C [12]) and quinine sulfate in 0.05 M H_2SO_4 (Φ_r=0.546 at 25 °C [13, 14]) were used as references.

$$\Phi_s = \frac{A_r F_s n_s^2}{A_s F_r n_r^2} \Phi_r \tag{1}$$

where A is the absorbance at the excitation wavelength, F the integrated emission area and n the refraction index of the solvents used. Subscripts refer to the reference (r) or sample (s) compound.

The steady-state fluorescence anisotropy, r, is calculated by

$$r = \frac{I_{VV} - G I_{VH}}{I_{VV} + 2 G I_{VH}} \tag{2}$$

where I_{VV} and I_{VH} are the intensities of the emission spectra obtained with vertical and horizontal polarization, respectively (for vertically polarized excitation light), and $G = I_{HV}/I_{HH}$ is the instrument correction factor, where I_{HV} and I_{HH} are the emission intensities obtained with vertical and horizontal polarization (for horizontally polarized excitation light).

Data analysis

Solvatochromic shifts were described by the Lippert-Mataga Eq. (3), which relates the energy difference between absorption and emission maxima to the orientation polarizability, [15, 16]

$$\overline{v}_{abs} - \overline{v}_{fl} = \frac{1}{4\pi\varepsilon_0} \frac{2\Delta\mu^2}{hcR^3} \Delta f + const \tag{3}$$

where $\overline{v}_{abs}$ is the wavenumber of maximum absorption, $\overline{v}_{fl}$ is the wavenumber of maximum emission, $\Delta\mu = \mu_e - \mu_g$ is the difference in the dipole moment of solute molecule between excited (μ_e) and ground (μ_g) states, R is the cavity radius (considering the fluorophore a point dipole at the center of a spherical cavity immersed in the homogeneous solvent), and Δf is the orientation polarizability given by (Eq. 4):
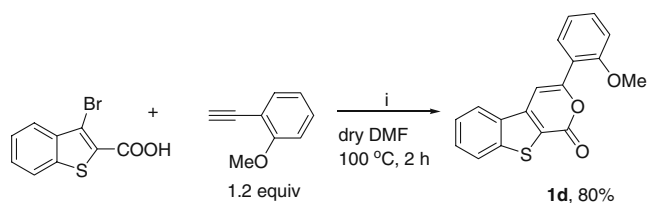
$$\Delta f = \frac{\varepsilon - 1}{2\varepsilon + 1} - \frac{n^2 - 1}{2n^2 + 1}, \tag{4}$$

where ε is the static dielectric constant and n the refractive index of the solvent.

Fluorescence anisotropy components (I_{VV} and $G \cdot I_{VH}$) were globally fitted to two sums of lognormal components (Eqs. 5 and 6) [17], each sum characterized by a fitted anisotropy value,

$$\begin{aligned} I_{VV} = \sum_i &\frac{A_{1i}}{\left(\lambda - (\lambda_{max})_{1i} + a_{1i}\right)} \exp\left(-c_{1i}^2\right) \\ &\exp\left\{-\frac{1}{2c_{1i}^2}\left[\ln\left(\frac{\lambda - (\lambda_{max})_{1i} + a_{1i}}{b_{1i}}\right)\right]^2\right\} + \\ &+ \sum_i \frac{A_{2i}}{\left(\lambda - (\lambda_{max})_{2i} + a_{2i}\right)} \exp\left(-c_{2i}^2\right) \\ &\exp\left\{-\frac{1}{2c_{2i}^2}\left[\ln\left(\frac{\lambda - (\lambda_{max})_{2i} + a_{2i}}{b_{2i}}\right)\right]^2\right\} \end{aligned} \tag{5}$$

$$\begin{aligned} G \cdot I_{VH} = \sum_i &\frac{A'_{1i}}{\left(\lambda - (\lambda_{max})_{1i} + a_{1i}\right)} \exp\left(-c_{1i}^2\right) \\ &\exp\left\{-\frac{1}{2c_{1i}^2}\left[\ln\left(\frac{\lambda - (\lambda_{max})_{1i} + a_{1i}}{b_{1i}}\right)\right]^2\right\} + \\ &+ \sum_i \frac{A'_{2i}}{\left(\lambda - (\lambda_{max})_{2i} + a_{2i}\right)} \exp\left(-c_{2i}^2\right) \\ &\exp\left\{-\frac{1}{2c_{2i}^2}\left[\ln\left(\frac{\lambda - (\lambda_{max})_{2i} + a_{2i}}{b_{2i}}\right)\right]^2\right\} \end{aligned}, \tag{6}$$

i) PdCl$_2$(PPh$_3$)$_2$ (5 mol%) CuI (3 mol%), NEt$_3$ (3 equiv.)

Scheme 1 Synthesis of compound **1d**

where A (or A') is the maximum intensity at wavelength λ_{max} and the parameters a, b and c are given by [17]

$$c = \ln(\rho) / \sqrt{2\ln(2)} \quad b = H\frac{\rho}{\rho^2-1}\exp(c^2) \quad a = H\frac{\rho}{\rho^2-1} \quad (7)$$

where H is the half-width of the band and ρ is the skewness. The lognormal function sums account for the vibrational structure of compound spectrum. The components (1 and 2) have two different fitted anisotropy values, r_1 and r_2, given by

$$r_1 = \frac{A_{1i} - A'_{1i}}{A_{1i} + 2A'_{1i}} \text{ and } r_2 = \frac{A_{2i} - A'_{2i}}{A_{2i} + 2A'_{2i}}, \quad (8)$$

due to the additivity law of anisotropy [18],

$$r = \sum_i \frac{I_i}{I_{total}} r_i \quad (9)$$

with

$$r_i = \frac{(I_i)_{VV} - G(I_i)_{VH}}{(I_i)_{VV} + 2G(I_i)_{VH}}. \quad (10)$$

Therefore,

$$A'_{1i} = A_{1i}\left(\frac{1-r_1}{1+2r_1}\right) \text{ and } A'_{2i} = A_{2i}\left(\frac{1-r_2}{1+2r_2}\right). \quad (11)$$

Results and discussion

Synthesis of compound **1d**

As referred above, compound **1d** was prepared in this work for comparison with compounds **1a–c** which were already prepared by some of us in a previous work [4], using the same method (Scheme 1).

Compound **1d** was prepared in an excellent yield by a *tandem* one-pot Pd/Cu catalyzed Sonogashira reaction of the 3-bromobenzo[*b*]thiophene-2-carboxylic acid with the 2-methoxyphenylacetylene followed by an intramolecular cyclization on the intermediate involving the carboxyl group and the triple bond [4].

Photophysical properties of compounds **1a-d** in homogeneous solution

The absorption and fluorescence properties of compounds **1a**, **1b**, **1c** and **1d** were studied in several solvents. The maximum absorption (λ_{abs}) and emission wavelengths (λ_{em}), molar extinction coefficients (ε) and fluorescence quantum yields (Φ_F) of the four compounds are presented in Table 1. The normalized fluorescence spectra of compounds **1a–d** are shown in Fig. 2. Examples of absorption spectra are displayed as insets.

The effect of solvent in the absorption spectrum of these compounds is generally small (insets of Fig. 2 and Table 1). Despite this, a red shift of the lowest energy absorption maximum can be observed with increasing solvent polarity, thus indicating that a $\pi \rightarrow \pi^*$ transition is involved. The molar extinction coefficients at absorption maxima are high ($\varepsilon > 10^4$ M^{-1} cm^{-1}), confirming this assumption.

In fluorescence spectra, significantly higher red shifts for all compounds can be observed from cyclohexane to more polar solvents, indicating that solvent relaxation after photoexcitation plays an important role. In polar solvents, a loss of vibrational structure is also detected (Fig. 2), more significant for compound **1c**, that presents completely non-structured emission bands in the more polar environments. This behavior is usually related to an intramolecular charge transfer (ICT) mechanism and/or to specific solvent effects [15].

The red shifts in emission are larger for the compounds with the electron-donating (EDG) OCH$_3$ group, especially for compound **1c** (26 nm from cyclohexane to DMSO). Compounds **1a** and **1b** exhibit smaller red shifts, which may be due to the dual character of the F atom, which is an EDG by mesomeric effect (+M) and an electron-withdrawing group (EWG) by inductive effect (-I). A similar behavior was already observed in tetracyclic lactams previously obtained by us, bearing this type of substituents [19].

The Lippert-Mataga plots (Eq. 3) for compounds **1a–d** (Fig. 3) display a high linearity for all compounds in the solvents studied. Therefore, specific solute–solvent interactions like hydrogen bonding are not detectable by deviations of linearity in the Lippert-Mataga plots.

From *ab initio* molecular quantum chemistry calculations, the cavity radius (R) and the ground state dipole moment (μ_g) were determined for the four compounds (Table 2), through an optimized structure provided by GAMESS software [21], using a RHF/3-21G(d) basis set [22] (Fig. 4). The optimized geometries show that molecules **1a** and **1c** are roughly planar, while in compounds **1b** and **1d** the fluorophenyl and the methoxyphenyl groups are out of the plane of the benzothienopyran-1-one moiety. The excited state dipole moments, μ_e, estimated from the Lippert-Mataga plots (Table 2), point to the presence of an intramolecular

Table 1 Maximum absorption (λ_{abs}) and emission wavelengths (λ_{em}), molar extinction coefficients (ε) and fluorescence quantum yields (Φ_F) for compounds 1a–d in several solvents

Solvent	λ_{abs}/nm ($\varepsilon/10^4 M^{-1} cm^{-1}$)				λ_{em}/nm				Φ_F			
	1a	1b	1c	1d	1a	1b	1c	1d	1a [a]	1b [a]	1c [b]	1d [b]
Cyclohexane	363 (1.23); 275 (2.03)	361 (1.57); 274 (3.16)	372 (1.70); 283 (2.88)	366 (1.36); 274 (2.57)	418	409	433	422	0.002	0.005	0.006	0.009
Dioxane	365 (1.25); 277 (2.67)	365 (2.17); 277 (4.12)	374 (1.89); 266 (3.03)	367 (1.66); 276 (2.09)	422	415	440	426	0.006	0.013	0.020	0.016
Dichloromethane	366 (1.72); 277 (3.78)	363 (1.46); 276 (3.39)	376 (1.40); 285 (2.75)	371 (1.30); 276 (2.48)	425	417	449	434	0.005	0.014	0.022	0.020
Dimethylformamide	367 (1.36)[c]	363 (1.40)[c]	378 (2.06); 286 (2.75)	370 (1.82); 278 (1.73)	427	419	456	437	0.010	0.012	0.039	0.015
Dimethylsulfoxide	369 (1.50)[c]	363 (1.70)[c]	381 (2.29); 286 (2.93)	372 (1.51); 279 (1.61)	429	420	459	438	0.012	0.016	0.068	0.030
Acetonitrilo	366 (1.04); 276 (2.06)	360 (1.29); 276 (3.39)	373 (1.23); 282 (2.61)	367 (1.71); 284 (3.41)	425	416	452	433	0.004	0.008	0.021	0.012
Ethanol	366 (1.57); 277 (3.67)	362 (1.30); 275 (2.94)	377 (1.77); 284 (3.63)	370 (1.49); 276 (2.90)	426	418	456	435	0.007	0.012	0.040	0.022
Methanol	367 (1.58); 277 (3.69)	363 (1.09); 275 (2.58)	377 (1.43); 283 (2.69)	370 (1.51); 275 (3.27)	427	420	458	437	0.006	0.012	0.047	0.023

[a] Relative to anthracene in ethanol ($\Phi_r = 0.27$ [12])

[b] Relative to quinine sulfate in 0.05 M H_2SO_4 ($\Phi_r = 0.546$ [13, 14])

[c] *Solvent cut-offs*: Dimethylformamide: 275 nm; Dimethylsulfoxide: 270 nm

charge transfer (ICT) mechanism, especially for compound **1c**. Twisted intramolecular charge transfer states (TICT) usually exhibit higher excited state dipole moments ($\geq$ 20 D) [23] than those here obtained.

Figure 5 reports the representation of HOMO and LUMO molecular orbitals for the four compounds. In all compounds, the HOMO-LUMO transition causes an increase in the electronic density of the O atom of the pyranone ring, especially in the case of compound **1c**. It can be observed that the HOMO-LUMO transition of compound **1c** exhibits a charge transfer from the oxygen atom of the methoxyphenyl group to the aromatic ring system,

Fig. 2 Normalized fluorescence (at peak of maximum emission) spectra of compounds **1a–d** in several solvents: cyclohexane (− − −); dioxane (······); dichloromethane (—); dimethylformamide (........); dimethylsulfoxide (− · · −); acetonitrile (- - - - -); ethanol (− · − · −); methanol (− · − · − · −). Insets: Absorption spectra of solutions of compounds **1a–d** in dichloromethane and in ethanol, as examples. **A** Compound **1a** (7×10^{-6} M solutions for fluorescence, $\lambda_{exc} = 360$ nm, and 2.4×10^{-5} M for absorption); **B** Compound **1b** (4×10^{-6} M solutions for fluorescence, $\lambda_{exc} = 360$ nm, and 2.5×10^{-5} M for absorption); **C** Compound **1c** (4×10^{-6} M solutions for fluorescence, $\lambda_{exc} = 370$ nm, and 2×10^{-5} M for absorption); **D** Compound **1d** (4×10^{-6} M solutions for fluorescence, $\lambda_{exc} = 370$ nm, and 2×10^{-5} M for absorption)
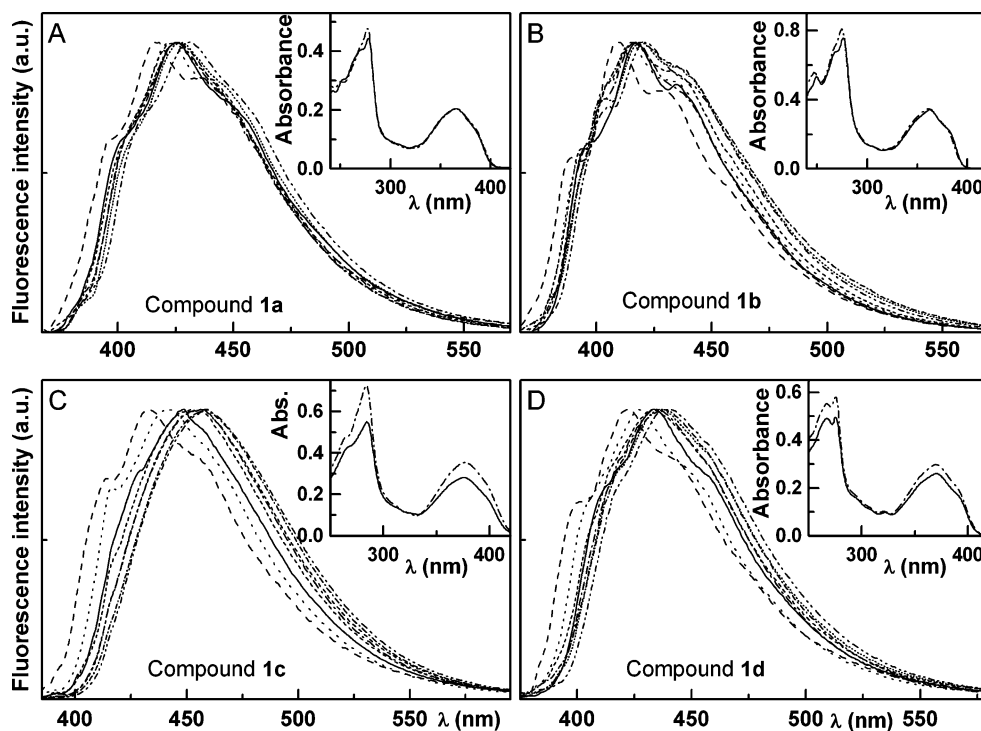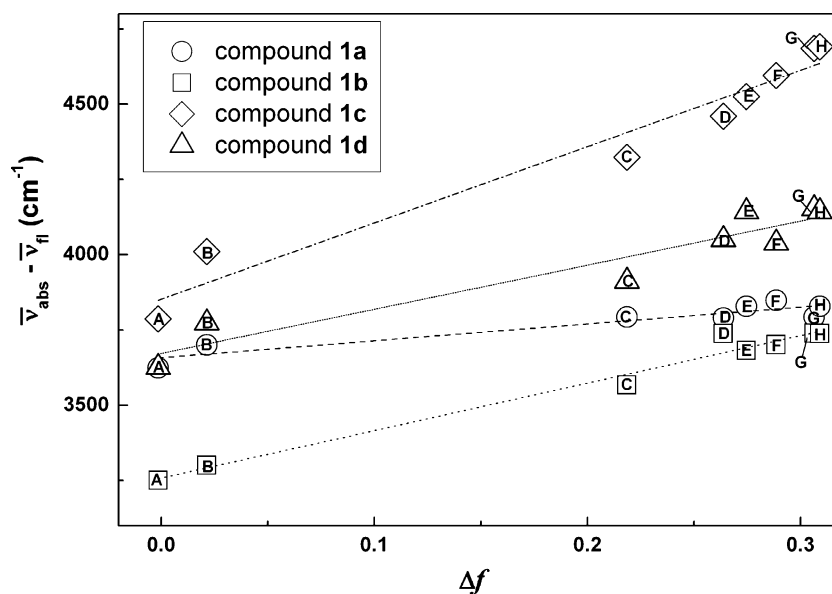
Fig. 3 Lippert-Mataga plots for compounds **1a**, **1b**, **1c** and **1d**. *A*: cyclohexane; *B*: dioxane; *C*: dichloromethane; *D*: dimethylsulfoxide; *E*: dimethylformamide; *F*: ethanol; *G*: acetonitrile; *H*: methanol (values of ε and n were obtained from ref. [20])
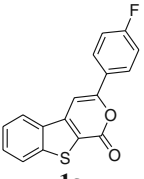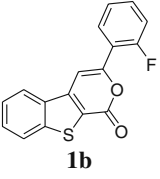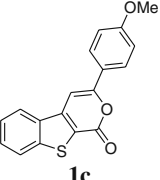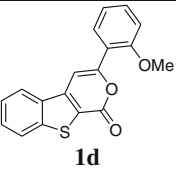
confirming the ICT character of the excited state. The effect is significantly lower for compound **1d**. Comparing compounds **1a** and **1b**, the F atom presents higher electronic density in compound **1a**, which decreases slightly upon HOMO-LUMO transition. It can also be observed that the carbon atom bound to fluorine decreases its electronic density upon HOMO-LUMO transition in compound **1a**, the opposite occurring in compound **1b**.

All compounds **1a**–**d** present low fluorescence quantum yields in all solvents ($\Phi_F \leq 6.8\%$, Table 1). Fluorescence quantum yields are very low ($\Phi_F < 2\%$) for compounds with a F substituent (**1a** and **1b**). For compounds with a

Table 2 Cavity radius (R) and ground state dipole moments (μ_g), obtained from theoretical calculations, and excited state dipole moments (μ_e) calculated from the Lippert-Mataga plots

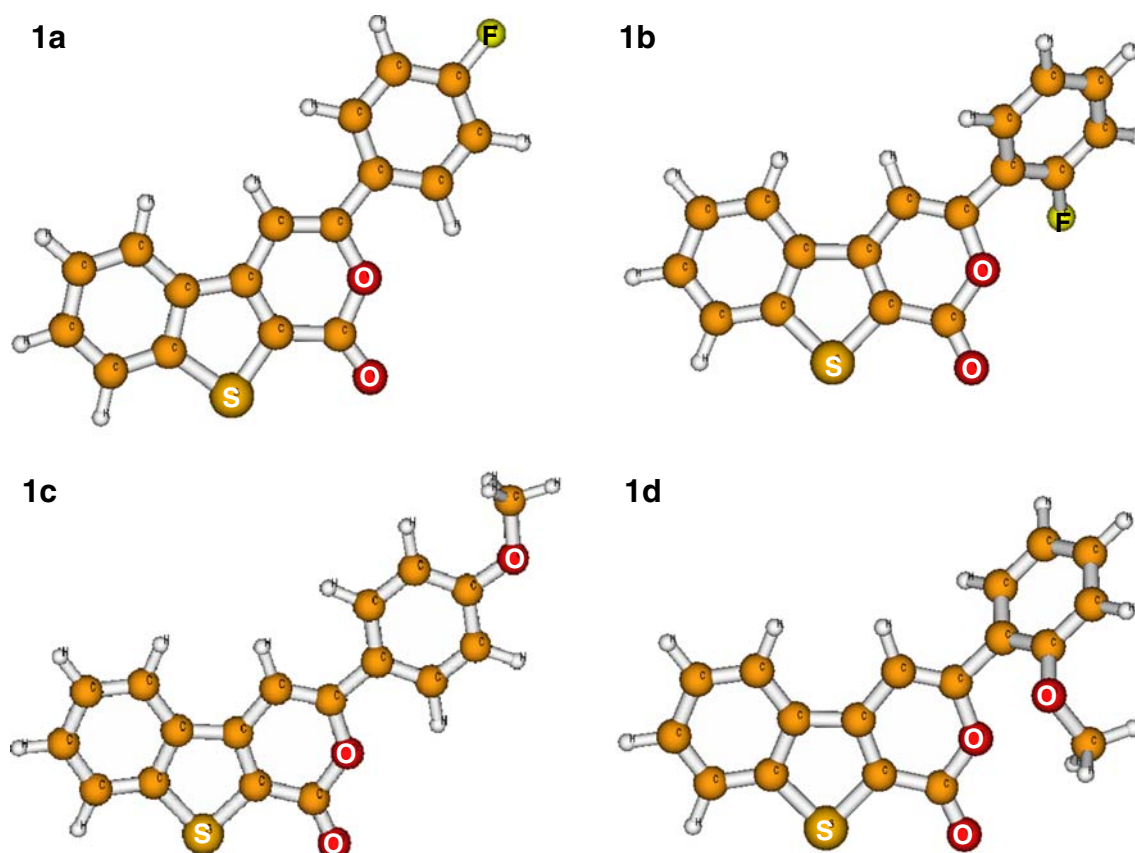| Compound	Cavity radius, R (Å)	Ground state dipole moment, μ_g (D)	Excited state dipole moment, μ_e (D)
1a	5.3	6.1	8.9
1b	5.8	7.6	13.1
1c	6.3	7.9	15.8
1d	6.1	5.1	10.8

Fig. 4 Optimized structures of compounds **1a**, **1b**, **1c** and **1d** (obtained by GAMESS software), with the indication of S, O and F atoms

methoxy substituent (**1c** and **1d**), Φ_F values are generally higher, especially in polar solvents. The low values of fluorescence quantum yield observed for these compounds are due to the presence of the S atom in the thiophene ring, which may promote the intersystem crossing process by enhancement of spin–orbit coupling interaction [15, 24], as observed for other molecules which include a thiophene ring [1, 19]. The expected formation of hydrogen bonds of compounds **1a**–**d** with protic solvents was not inferred from deviations of the Lippert-Mataga plots (Fig. 3) and, if they occur, do not influence the Φ_F values in alcohols (Table 1).

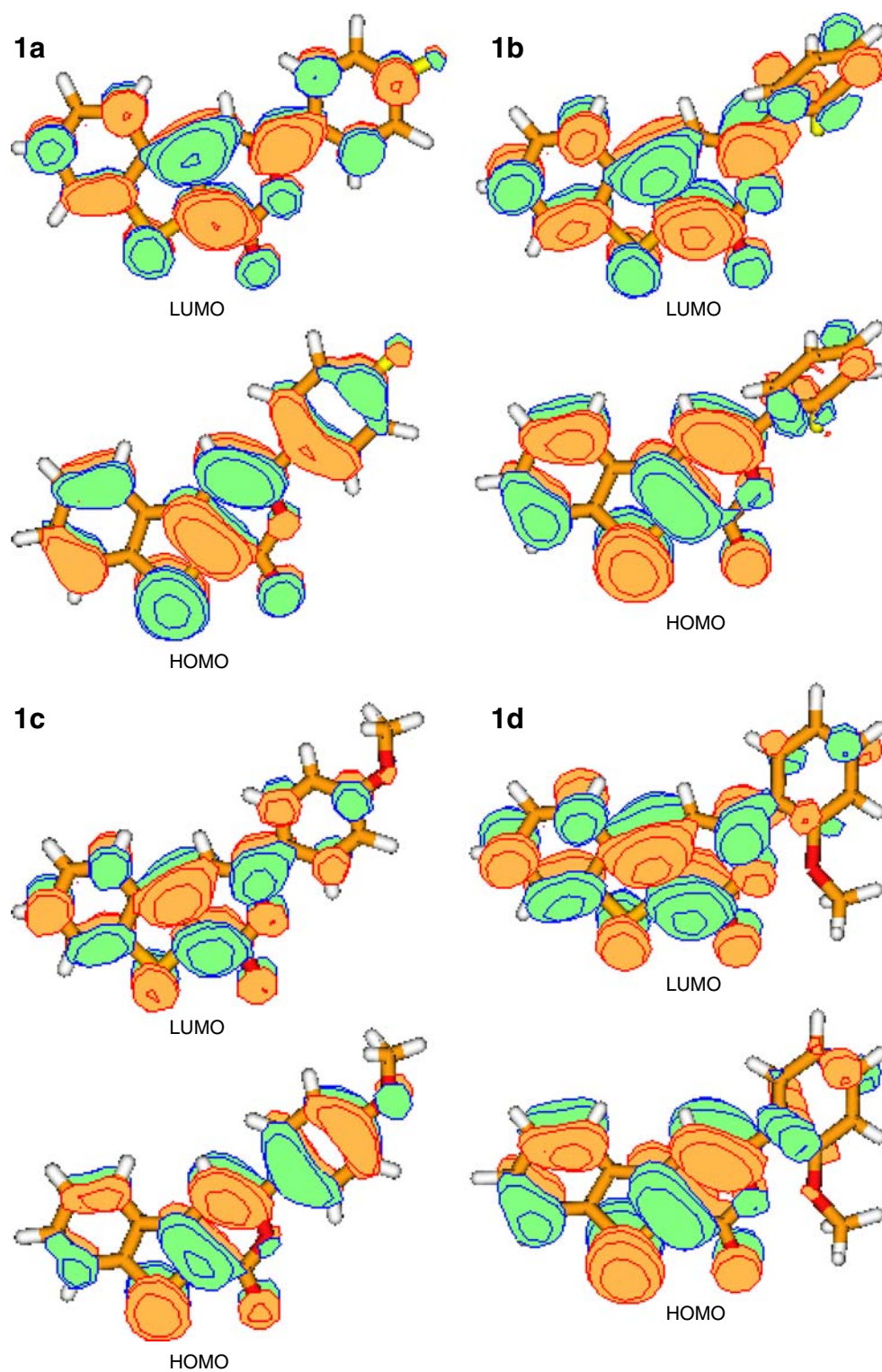Interaction of compounds **1a**–**d** with lipid membranes

Due to their promising antitumoral activity [4], photophysical studies of compounds **1a**–**d** incorporated in lipid vesicles were also performed. These experiments are important to evaluate their location in liposomes pointing to drug delivery applications.

Different types of lipid molecules, Egg-PC, DPPC and DODAB, were used for the vesicles preparation. Egg-PC is a natural phospholipid mixture, where all molecules have the same polar head group (phosphatidylcholine) but several hydrocarbon chains, differing in length and degree of unsaturation. Egg-PC main components are 16:0 PC, 18:0 PC and 18:1 PC [25]. Considering DPPC (16:0 PC) and DODAB, it is known that at room temperature, both lipids are in the ordered gel phase, where the hydrocarbon chains are fully extended and closely packed. Above the melting transition temperature, 41 °C for DPPC [8] and 45 °C for DODAB [9], these lipids attains the disordered liquid-crystalline phase.

The emission spectra of compounds **1a**–**d** in lipid membranes are displayed in Fig. 6. Compound **1a** (Fig. 6A) exhibits a composed spectrum in lipids at the gel phase (DODAB and DPPC at 25 °C), showing the existence of two emission bands (with maxima near 420 nm and 438 nm, Table 3), pointing to the existence of two different locations of **1a** molecules in these rigid lipid membranes. At the liquid-crystalline phase (both DPPC and DODAB at 55 °C and Egg-PC at 25 °C), only one emission band is observed, with very slight differences between the three lipids. The maximum emission wavelengths in this fluid phase (Table 3) are similar to the lower energy maximum of the compound in lipids at the gel phase. A distinct behavior is observed for compound **1b**, where the position and shape of the emission bands are similar in all lipids either at 25 °C or at 55 °C. A decrease of the shoulder at the higher energy region is

Fig. 5 Representation of
HOMO (*lower*) and LUMO
(*upper*) molecular orbitals of
compounds **1a–d**

For compounds **1c** and **1d** (Fig. 6C and D, respectively)
a structured emission is observed in Egg-PC, especially for
compound **1d**. In DPPC and DODAB, the emission bands
of both compounds are basically non-structured and, in
some cases, seem clearly to be composed of two emissions.
For compound **1c**, a significant spectral shift is observed
between the different lipid membranes. The maximum

observed in DODAB, especially in the fluid phase (Fig. 6B).
The maximum emission wavelengths indicate an environ-
ment of moderate polarity, similar to dioxane and acetonitrile
(Tables 1 and 3). In homogeneous solution, the effect of the
temperature increase in the fluorescence of these compounds
is a *ca.* 40% reduction and a very small blue shift (1–2 nm)
between 25 °C and 55 °C.

Fig. 6 Normalized fluorescence spectra of compounds **1a**–**d** in lipid membranes: Egg-PC at 25 °C (—); DPPC gel phase at 25 °C (− − −); DPPC liquid-crystalline phase at 55 °C (− · − · −); DODAB gel phase at 25 °C (· · · · · ·); DODAB liquid-crystalline phase at 55 °C (........). Insets: Fluorescence anisotropy spectrum of compounds **1a**–**d** in DPPC at gel phase (25 °C), as an example. **A** Compound **1a** ($\lambda_{exc}=$ 360 nm); **B** Compound **1b** ($\lambda_{exc}=360$ nm); **C** Compound **1c** ($\lambda_{exc}=370$ nm); **D** Compound **1d** ($\lambda_{exc}=370$ nm)
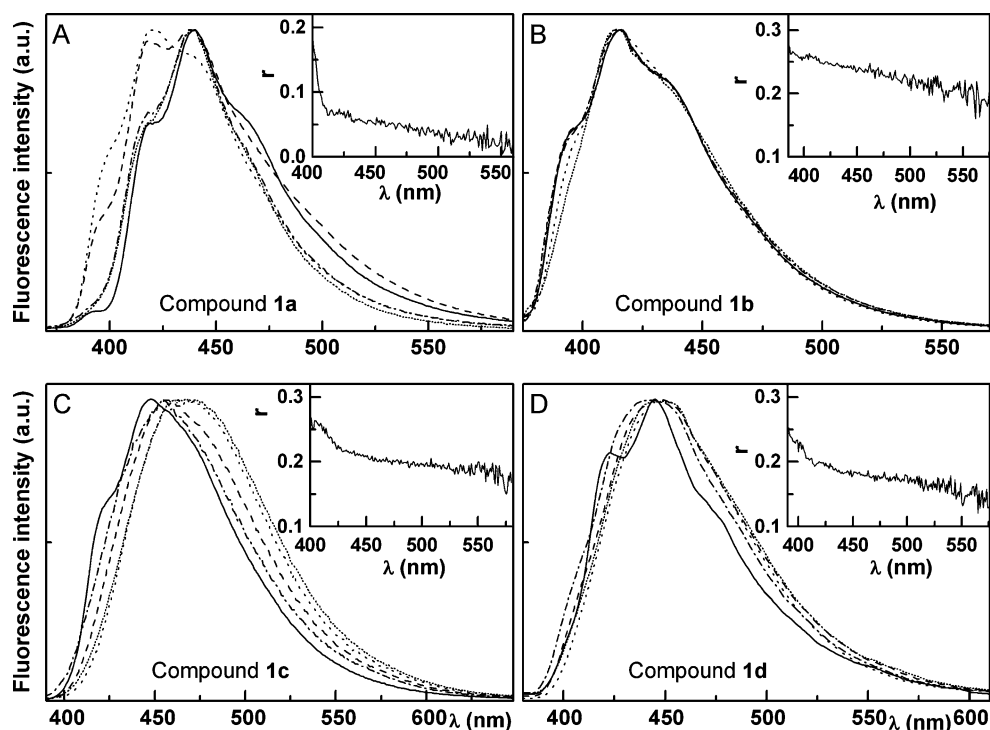
emission wavelength in Egg-PC is similar to that in dichloromethane, while for DODAB a more hydrated environment is predicted. For compound **1d**, the emission maxima in all lipids are similar to the observed in ethylene glycol, pointing also to a hydrated location of this compound in lipid vesicles.

In order to obtain further information about the behavior of these molecules in lipid membranes, fluorescence (steady-state) anisotropy measurements were performed. The average fluorescence steady-state anisotropies ($\bar{r}$) and fluorescence quantum yields of the four compounds in lipid vesicles are shown in Table 3. Fluorescence anisotropy values in ethylene glycol at room temperature were also determined for comparison, being similar for all molecules. For each compound, an example of fluorescence anisotropy spectrum is displayed as inset in Fig. 6. Notable variations

with emission wavelength are observed for compound **1a** (inset of Fig. 6A), while the variations are smaller for compounds **1c**, **1d** and **1b** (inset of Fig. 6B–D). In ethylene glycol, the steady-state fluorescence anisotropy is constant with wavelength for all compounds. The behavior observed in lipid membranes points to the existence of two emitting species, corresponding to compound locations in different environments.

Figures 7 and 8 display an example of the fit of anisotropy components, I_{VV} and $G \cdot I_{VH}$ (Eqs. 5 and 6), and the fitting to the anisotropy curve, as well as the respective spectral contributions recovered from the fitting. The results are given in Table 4.

For all compounds, two components were recovered, one with higher anisotropy (r_1) and lower maximum

Table 3 Average steady-state fluorescence anisotropy ($\bar{r}$) values, fluorescence quantum yields and maximum emission wavelengths (λ_{em}) of compounds **1a**–**d** in lipid membranes. Values in ethylene glycol at room temperature are also shown for comparison

	Compound **1a**			Compound **1b**			Compound **1c**			Compound **1d**		
	λ_{em} /nm	Φ_F [a]	$\bar{r}$	λ_{em} /nm	Φ_F [a]	$\bar{r}$	λ_{em} /nm	Φ_F [b]	$\bar{r}$	λ_{em} /nm	Φ_F [b]	$\bar{r}$
DPPC (25 °C)	419; 438	0.034	0.089	416	0.011	0.234	459	0.042	0.203	448	0.030	0.194
DPPC (55 °C)	438	0.013	0.065	415	0.004	0.185	457	0.010	0.192	444	0.008	0.190
DODAB (25 °C)	421	0.084	0.188	415	0.013	0.210	467	0.054	0.173	449	0.031	0.189
DODAB (55 °C)	439	0.047	0.075	414	0.005	0.140	469	0.017	0.161	448	0.011	0.167
Egg-PC (25 °C)	440	0.024	0.066	416	0.006	0.231	449	0.022	0.229	424; 445	0.015	0.212
Ethylene glycol (25 °C)	431	–	0.276	421	–	0.272	465	–	0.240	444	–	0.264

[a] Relative to anthracene in ethanol ($\Phi_r=0.27$ at 25 °C [12])

[b] Relative to quinine sulfate in 0.05 M H_2SO_4 ($\Phi_r=0.546$ at 25 °C [13, 14])

Fig. 7 Fit of compound **1a** in DODAB gel phase (25 °C). **A** I_{VV} component and fitted curve; **B** $G \cdot I_{VH}$ component and fitted curve; **C** Recovered spectral components from the fitting procedure; **D** Fluorescence steady-state anisotropy and recovered curve (calculated from the recovered components)
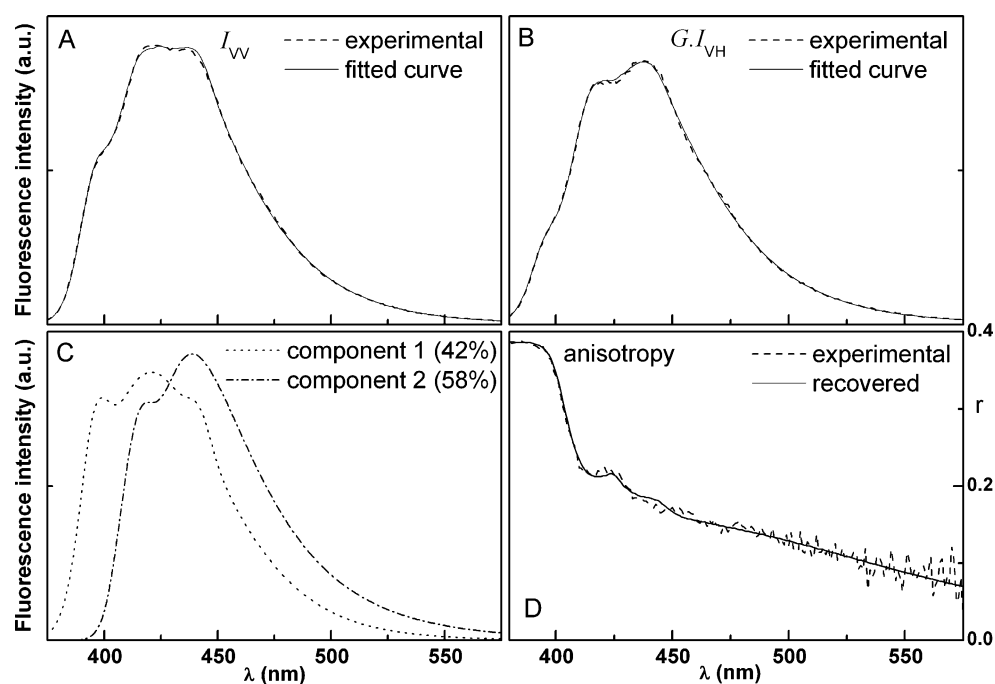
emission wavelength (λ_1), corresponding to compound molecules located deeper in the lipid membrane, and another corresponding to a more hydrated environment (higher emission wavelength, λ_2, and lower anisotropy, r_2). The fraction of the first component, f_1 (corresponding to the fraction of spectral area), is also presented. In general, the microviscosity decreases from the interface to the interior of the membrane [26, 27], with a more pronounced variation when the membrane is in the liquid-crystalline phase [27]. Thus, the recovered anisotropy values for the two compound locations are in opposite direction to that given by the spectral band positions. This can be explained by the observed increase in the fluorescence quantum yield with solvent polarity (Table 1). The absorption spectra exhibit a very low dependence on solvent polarity (insets of Fig. 2). From the Strickler-Berg relation [18, 28], it can be concluded that the radiative lifetime, τ_r, is mainly invariant with polarity. Therefore, a higher Φ_F value results from an increase of the excited-state lifetime. This, in turn, contributes to a decrease in fluorescence anisotropy, as the excited

Fig. 8 Fit of compound **1d** in DODAB gel phase (25 °C). **A** I_{VV} component and fitted curve; **B** $G \cdot I_{VH}$ component and fitted curve; **C** Recovered spectral components from the fitting procedure; **D** Fluorescence steady-state anisotropy and recovered curve (calculated from the recovered components)
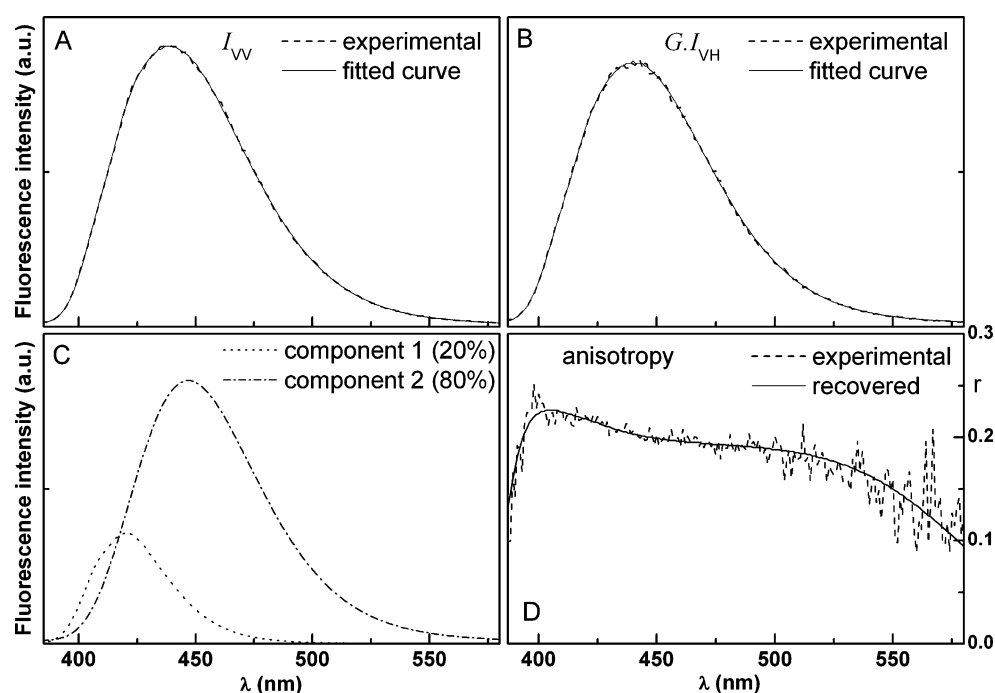
Table 4 Steady-state fluorescence anisotropy (r) of the two anisotropy components, weights of the first component (f_1) and respective maximum emission wavelengths (λ_{max}) for compounds **1a–d** in lipid membranes

	Compound **1a**					Compound **1b**					Compound **1c**					Compound **1d**				
	f_1	r_1	λ_1 (nm)	r_2	λ_2 (nm)	f_1	r_1	λ_1 (nm)	r_2	λ_2 (nm)	f_1	r_1	λ_1 (nm)	r_2	λ_2 (nm)	f_1	r_1	λ_1 (nm)	r_2	λ_2 (nm)
DPPC (25 °C)	0.38	0.147	422	0.054	448	0.58	0.256	414	0.231	442	0.27	0.260	425	0.188	455	0.19	0.230	417	0.177	446
DPPC (55 °C)	0.08	0.146	417	0.022	439	0.51	0.219	406	0.187	440	0.47	0.278	439	0.173	456	0.18	0.238	418	0.175	442
DODAB (25 °C)	0.42	0.287	422	0.057	439	0.58	0.248	410	0.190	444	0.37	0.256	429	0.164	463	0.20	0.250	420	0.194	447
DODAB (55 °C)	0.13	0.128	419	0.029	439	0.60	0.222	409	0.109	440	0.50	0.231	440	0.132	464	0.21	0.221	422	0.163	444
Egg-PC (25 °C)	0.06	0.130	417	0.014	440	0.54	0.247	414	0.229	440	0.31	0.258	424	0.238	455	0.32	0.250	420	0.228	442

compound has more time to rotate leading to a depolarization of its fluorescence.

Compound **1a** locates mainly in a very hydrated environment (λ_2 values higher than λ_{max} observed in methanol), while compound **1b** preferential location is deeper inside the lipid membrane, as the component with lower maximum emission wavelength (406–414 nm) is dominant ($f_1 > 0.50$). For compounds **1a** and **1b**, similar environments (as inferred from the maximum emission wavelengths) show very distinct anisotropy values for component 2 (Table 4), r_2 value being especially low for compound **1a**. The different geometry (*vd*. Fig. 4) of both compounds cannot explain this distinct behavior, as compounds **1c** and **1d** which have also different geometries do not show similar variations in anisotropy values. This peculiar behavior of compound **1a** indicates that some of its molecules locate at the outer part of the liposome interface, with a fluidity approaching that of water.

Upon transition from the gel (25 °C) to the liquid-crystalline (55 °C) phase (for DPPC and DODAB), compound **1a** relocates to a more hydrated environment, as the f_1 value strongly decreases. The opposite seems to happen for compound **1c**, where f_1 clearly increases at 55 °C. Therefore, compounds with a planar geometry (**1a** and **1c**) have higher mobility in the lipid vesicles when phase transition occurs.

Liposomes have been widely used to deliver anticancer agents, in order to reduce the toxic effects of the drugs or to increase the drug circulation time and effectiveness [29]. The studies described here are important for the incorporation of the new potential antitumoral benzothienopyran-1-ones in liposomes for future controlled drug delivery applications.

Conclusions

The four new potential antitumoral compounds, 3-arylbenzothieno[2,3-*c*]pyran-1-ones, show a solvent sensitive emission, with significant red shifts in polar solvents for the methoxylated compounds. Compound **1c** exhibits the higher fluorescence quantum yields in all solvents studied. The estimated excited state dipole moments point to an ICT character of the excited state, more pronounced for compound **1c**, confirmed by molecular quantum chemistry calculations.

Photophysical studies of the compounds incorporated in liposomes of DPPC, DODAB and Egg-PC indicate that all the compounds exhibit two different locations, one due to a deep penetration in the lipid membrane and other corresponding to a more hydrated environment. Compounds with a planar geometry (**1a** and **1c**) have higher mobility in the lipid vesicles when phase transition occurs.

Considering the already tested anti-proliferative activity of human tumor cell lines exhibited by these molecules, the

results obtained here are important for future drug delivery applications using liposomes.

References

1. Queiroz M-JRP, Castanheira EMS, Pinto AMR, Ferreira ICFR, Begouin A, Kirsch G (2006) Synthesis of the first thieno-δ-carboline. Fluorescence studies in solution and in lipid vesicles. J Photochem Photobiol A: Chem 181:290–296

2. Castanheira EMS, Abreu AS, Carvalho MSD, Queiroz M-JRP, Ferreira PMT (2009) Fluorescence studies on potential antitumoral heteroaryl and heteroannulated indoles in solution and in lipid membranes. J Fluorescence 19:501–509

3. Castanheira EMS, Abreu AS, Queiroz M-JRP, Ferreira PMT, Coutinho PJG, Nazareth N, Nascimento MS-J (2009) Fluorescence properties of a potential antitumoral benzothieno[3, 2-b]pyrole in solution and lipid membranes. J Photochem Photobiol A: Chem 206:220–226

4. Queiroz M-JRP, Calhelha RC, Vale-Silva LA, Pinto E, Nascimento MS-J (2009) Synthesis of novel 3-(aryl)benzothieno[2, 3-c]pyran-1-ones from Sonogashira products and intramolecular cyclization: antitumoral activity evaluation. Eur J Med Chem 44:1893–1899

5. Lasic DD (1995) In: Lasic DD, Barenholz Y (eds) Handbook of nonmedical applications of liposomes: from gene delivery and diagnostic to ecology, vol IV. CRC, New York, pp 1–32

6. Lasic DD, Ruff D (1998) In: Lasic DD, Papahadjoupoulos D (eds) Medical applications of liposomes. Elsevier, Netherlands, pp 353–394

7. Pedroso de Lima MC, Simões S, Pires P, Faneca H, Düzgünes N (2001) Cationic lipid-DNA complexes in gene delivery: from biophysics to biological applications. Adv Drug Deliv Rev 47:277–294

8. Lentz BR (1989) Membrane "fluidity" as detected by diphenyl-hexatriene probes. Chem Phys Lipids 50:171–190

9. Feitosa E, Barreleiro PCA, Olofsson G (2000) Phase transition in dioctadecyldimethylammonium bromide and chloride vesicles prepared by different methods. Chem Phys Lipids 105:201–213

10. Demas JN, Crosby GA (1971) The measurement of photoluminescence quantum yields. A review. J Phys Chem 75:991–1024

11. Fery-Forgues S, Lavabre D (1999) Are fluorescence quantum yields so tricky to measure? A demonstration using familiar stationery products. J Chem Educ 76:1260–1264

12. Dawson WR, Windsor MW (1968) Fluorescence yields of aromatic compounds. J Phys Chem 72:3251–3260

13. Melhuish WH (1961) Quantum efficiencies of fluorescence of organic substances—effect of solvent and concentration of fluorescent solute. J Phys Chem 65:229–235

14. Meech SR, Phillips D (1983) Photophysics of some common fluorescence standards. J Photochem 23:193–217

15. Lakowicz JR (1999) Principles of fluorescence spectroscopy. Kluwer Academic/Plenum, New York

16. Mataga N, Kubota T (1970) Molecular interactions and electronic spectra. Marcel Dekker, New York

17. Siano DB, Metzler DE (1969) Band shapes of electronic spectra of complex molecules. J Chem Phys 51:1856–1861

18. Valeur B (2001) Molecular fluorescence—principles and applications. Wiley-VCH, Weinheim

19. Queiroz M-JRP, Castanheira EMS, Lopes TCT, Cruz YK, Kirsch G (2007) Synthesis of fluorescent tetracyclic lactams by a "one pot" three steps palladium-catalyzed borylation, Suzuki coupling (BSC) and lactamization. DNA and polynucleotides binding studies. J Photochem Photobiol A: Chem 190:45–52

20. Lide DR (ed) (2002) Handbook of chemistry and physics, 83rd edn. CRC, Boca Raton

21. Schmidt MW, Baldridge KK, Boatz JA, Elbert ST, Gordon MS, Jensen JH, Koseki S, Matsunaga N, Nguyen KA, Su S, Windus TL, Dupuis M, Montgomery JA (1993) General atomic and molecular electronic structure system. J Comput Chem 14:1347–1363

22. Jensen F (1999) Introduction to computational chemistry. Wiley, West Sussex

23. Grabowski ZR, Rotkiewicz K, Rettig W (2003) Structural changes accompanying intramolecular electron transfer: focus on twisted intramolecular charge-transfer states and structures. Chem Rev 103:3899–4031

24. Turro NJ (1978) Modern molecular photochemistry. Benjamin/Cummings, Menlo Park

25. Papahadjopoulos D, Miller N (1967) Phospholipid model membranes. I. Structural characteristics of hydrated liquid crystals. Biochim Biophys Acta 135:624–638

26. Tilley L, Thulborn KR, Sawyer WH (1979) An assessment of the fluidity gradient of the lipid bilayer as determined by a set of n-(9-anthroyloxy)fatty acids (n = 2, 6, 9, 12, 16). J Biol Chem 254:2592–2594

27. Bahri MA, Heyne BJ, Hans P, Seret AE, Mouithys-Mickalad AA, Hoebeke MD (2005) Quantification of lipid bilayer effective microviscosity and fluidity effect induced by propofol. Biophys Chem 114:53–61

28. Strickler SJ, Berg RA (1962) Relationship between absorption intensity and fluorescence lifetime of molecules. J Chem Phys 37:814

29. Banerjee R (2001) Liposomes: applications in medicine. J Biomater Appl 16:3–21